Draft version November 29, 2016
Preprint typeset using LaTeX style emulateapj v. 5/2/11

arXiv:1611.08746v1 [astro-ph.HE] 26 Nov 2016

EARLY IDENTIFICATION OF TYPE I SUPERNOVA LIGHT CURVES

W. David Arnett[1], Christopher Fryer[2], and Thomas Matheson[3]

Draft version November 29, 2016

ABSTRACT

We compare analytic light curves for SNIabc supernovae with recent high quality data from (1)) SN2011fe (Pereira, et al. 2013), (2) KSN2011b (Olling, et al. 2015), (3) the Palomar Transient Factory (PTF) and the La Silla-QUEST variability survey (LSQ) (Firth, et al. 2015), and (4) a type Ib, SN2008D (Modjaz, et al. 2008; Soderberg et al. 2008). We establish a reasonable bolometric conversion between Kepler supernovae and SN2011fe, a crude but instructive one for SN2008D, and discuss the implications of the smoothness of the light-curve for KSN2011b, as well as the meaning of the deviation of early luminosity from t^2 behavior. The good agreement of the analytic light curves (which necessarily assume mixing and which can reproduce the Phillips relation) and the observations of highest cadence and stability, are consistent with the occurrence of significant large-scale mixing during the explosion, possibly due to 3D effects (e.g., Rayleigh-Taylor and Richtmeyer-Meshkov instabilities) and consistent with spectrapolarimetry (Porter, et al. 2016). We illustrate how to separate the light curve of SN2008D, a type Ib (Bianco, et al. 2014) into thermal outburst (both break-out and dynamic acceleration) and radioactive components. The shape of a normalized light-curve can provide an indication of the *phase* of newly–discovered Type Ia supernovae, so that 3 early observations are mathematically sufficient to identify an event about 10–18 days prior to maximum, which has implications for survey telescopes such as LSST. We discuss the interpretation of the "opacity" in the analytic solution in terms of an equivalent integrated leakage rate for thermal photons. We derive a general relationship between extrema in the light curve and an arbitrary heating rate.

1. INTRODUCTION

Supernovae whose luminosity is primarily powered by the decay chains ^{56}Ni(e$^-,\nu$)^{56}Co, ^{56}Co(e$^-,\nu$)^{56}Fe and ^{56}Co(,e$^+\nu$)^{56}Fe have generic features. These are prominent in SNIa, and appear in SNIbc, that is, in both thermonuclear supernovae and those core-collapse supernovae which have lost their hydrogen envelopes (Arnett 1982, 1996).

Automated searches for supernovae are progressing to the point that it is desirable to have robust procedures to identify interesting objects early in their evolution, for subsequent follow–up observations. We compare theoretical light curves (Arnett 1982; Pinto & Eastman 2000a,b) to the best-observed SNIa to date, SN2011fe in M101, the Pinwheel galaxy (Pereira, et al. 2013), as well as to KSN2011b, the best of three SNIae (KSN 2011b,c; KSN2012a) detected at early times by the Kepler satellite (Olling, et al. 2015). For these supernovae we have bolometric (or near bolometric) light curves, so we may minimize issues of time-dependent atmospheric physics. This approach, which assumes three–dimensional (3D) incomplete mixing during the explosion (Arnett & Meakin 2016), is thus different from and a natural complement to a 1D, time–dependent non-LTE approach such as Blondin, et al. (2013); Dessart, et al. (2015, 2016). In addition the analytic solutions allow a quantitative and precise study of the light curve shapes.

[1] Steward Observatory, University of Arizona, 933 N. Cherry Avenue, Tucson AZ 85721
[2] Los Alamos National Laboratory, Los Alamos NM
[3] National Optical Astronomy Observatory, Tucson AZ

2. SHAPES OF SUPERNOVA LIGHT CURVES

2.1. *Light curves for SN2011fe*

If they are normalized to the luminosity at maximum light, supernova light curves of Type I have a characteristic shape, which is due to radioactive heating by gamma-rays and positrons, cooling by expansion, and cooling by radiative loss (Arnett 1982; Pinto & Eastman 2000a). Fig. 1 illustrates this both observationally for SN2011fe (Pereira, et al. 2013), and theoretically (Arnett 1982).

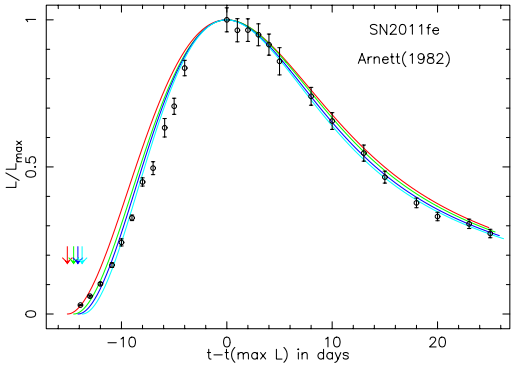

Figure 1. Comparison of normalized bolometric luminosity in analytic models (Arnett 1982) and SN2011fe (Pereira, et al. 2013). The analytic models plotted here allow for γ–ray escape, as did the original ones, by using the deposition estimate from Monte Carlo simulations of Colgate, Petschek & Kriese (1980). The four analytic curves are distinguished by a slightly different (10%) value for the p_2 parameter (see text); this is related to the relation between luminosity and light curve width (Phillips 1993). The curves are separately normalized at their own maximum light. The downward arrows indicate the beginning time of each light curve calculation.

The physical interpretation of the analytic solutions is slightly modified from Arnett (1982). The light curves begin *after* the explosion, and after shock emergence at the stellar surface. Three-dimensional instabilities in the flow, especially the Richtmeyer-Meshkov instability which is the Rayleigh-Taylor instability with gravity replaced by inertial forces (Swisher, et al. 2015), will give overturn and macroscopic but incomplete mixing. *This modifies any strict layering present in the ejecta*, such as found in many theoretical models of the progenitors.

Due to rapid expansion, adiabatic cooling converts thermal to kinetic energy, and soon almost all the supernova energy is contained in the velocity field (see Appendix B). The light curve develops due to subsequent heating by radioactive decay. Despite this change in interpretation, the theoretical light curves use identical parameters and mathematical methods to those used in the original paper, and are in this sense a prediction rather than a fit to the observational data. By normalizing the light curves to peak luminosity, the time derivatives of $L(t)$ become the natural diagnostics to use.

The four analytic curves (colored solid lines) in Fig. 1 differ in the value of the dimensionless parameter

$$p_2 = \tau_{Ni}/\tau_d, \tag{1}$$

which is the ratio of the decay time for Ni^{56} to the radiative diffusion time (the leakage time), where

$$\tau_d = \kappa_t M_{ej}/\beta c R(0), \tag{2}$$

and $\beta \approx 13.7$ is a dimensionless spatial integration constant which varys slowly in time (Arnett 1980), κ_t is the equivalent constant opacity, M_{ej} is the mass of ejected matter, c is the speed of light, and $R(0)$ is the value of the radius at the time after shock–breakout. The parameter p_2 is increased by steps of 10 percent, corresponding to a decrease in the ratio of $R(0)/(\kappa_t M_{ej})$. This gives a sequence which is similar to the Phillips relation (Phillips 1993); see §2.2 below.

The basic nature of the light curve may be naturally divided into three epochs: onset, rise to peak, and post–peak. At very early times ($t \leq -10$ days) the luminosity rises quadraticaly[4] with time ($d^2L/d^2t > 0$). The detailed structure of luminosity $L(t)$ is qualitatively correct here, but deviates in detail from the observations; this error is due in part to the coasting approximation[5], used in Arnett (1982) and in the "fireball model" of Riess, et al. (1999). *The approximation is unnecessary, and may be eliminated,* as we shall show quantitatively in a subsequent paper (see also Appendix B).

In this "coasting" or "fireball" approximation, the luminosity changes are due only to increasing area of the surface of emission. The radius is assumed to increase linearly with

[4] Eq. 46 in Arnett (1982) contains a typographical error: $\Gamma(x, y) \approx (xy)^2 \sim t^2$, not x^2 as printed. This error propagated to Arnett (1996), Eq. D.64. Only this limit is in error; the full equations are correct, and even with this error the time dependence of luminosity is quadratic.

[5] In 1982 there was too lttle data prior to peak light to make this an urgent issue.

time, so $L \propto t^2$. However, if the velocity grows (acceleration is positive) then luminosity increases with a higher power of time. For a constant radiative acceleration (constant flux at early times), $L \propto t^4$ and asymptotically approaches $L \propto t^2$. Thus $L \propto t^n$, where $n \sim 4 \rightarrow 2$, and n is slowly varying, purely from dynamics. In addition there may be effects related to the energy input differing from pure decay of uniformly distributed ^{56}Ni; see Piro & Nakar (2013).

Supernova time is commonly measured relative to peak luminosity rather than explosion time, so that $t \rightarrow t - t_{peak}$; this variable is easier to determine observationally. The early epoch, now at negative time t, is followed by a roughly linear rise in luminosity with time ($d^2L/dt^2 \approx 0$ and $dL/dt > 0$ over $-10 \leq t \leq -4$ days). The luminosity turns at peak (d^2L/dt^2 becomes negative and $dL/dt \approx 0$), and then begins to decline ($dL/dt < 0$ for $t \geq 0$). The downward arrows in Fig. 1 indicate the respective beginning times used for the calculation of the analytic light curves (Arnett 1982). Relaxation of the coasting approximation would shift these arrows earlier in time, improving agreement with the data.

Firth, et al. (2015) present an analysis of the early, rising light curves of 18 Type Ia supernovae (SNe Ia) discovered by the Palomar Transient Factory (PTF) and the La Silla-QUEST variability survey (LSQ). Fitting the early data to a power law in time results in a rise time of 18.98 ± 0.54 days and a power of $n = 2.44 \pm 0.13$. This was interpreted as "less Ni mixing", but also could be a natural outcome of relaxing the "coasting approximation", giving both $n > 2$ and earlier explosion ("bang") time relative to peak light. The suggestion of an increase in n with time ($dn/dt > 0$) would indicate that the early light curves are too complex for such simple dynamic arguments to capture (which suggest $dn/dt < 0$).

Firth, et al. (2015) find that the early light curve *does not correlate* with light curve shape or stretch. This is also seen in the analytic models; see Fig. 2 below and discussion following it.

Globally incomplete mixing (Arnett & Meakin 2016) would be expected from plume penetration without a return flow to complete a convective roll. Rayleigh-Taylor and Richtmeyer-Meshkov instabilities in the explosion and aftermath would give the early emergence of radioactivity seen in SN1987A, the composition heterogeneity seen in Cas A (Fesen & Milisavljevic 2016), and the filamentation seen in young supernova remnants. This sort of mixing is also seen in well–resolved 3D models of supernova explosions.

Table 1
Base model for SN2011fe

Variable	Symbol	Value
Mass ejected[a]	M_{ej}	$1.40 M_\odot$
Initial ^{56}Ni	$M_{Ni}(0)$	$0.60 M_\odot$
Initial radius	$R(0)$	1.0×10^{10} cm
Opacity	κ_t	0.10 cm^2 g^{-1}
Explosion energy	E_{sn}	1.3×10^{51} ergs

[a] Total stellar mass for SNIae.

Table 2
Initial[a] values of derived parameters

Variable	Symbol	Value
Velocity scale	v_{sc}	9.6594×10^8 cm s^{-1}
Expansion time	τ_h	10.353 s
Diffusion time	τ_d	6.7779×10^{10} s
Density	$\rho(0)$	6.64×10^2 g cm^{-3}
Temperature	$T(0,0)$	8.00×10^7 K
Optical depth	$\rho(0)\kappa_t R(0)$	6.64×10^{12}

[a] After shock emergence.

The astrophysical parameters chosen for the SN2011fe light curves are documented in Table 1. These determine the analytic light curve solutions mathematically.

The starting values (after shock emergence) for some of the important variables in the analytic models for SN2011fe are presented in Table 2.

2.2. *Absolute bolometric luminosity*

A more interesting challenge is to consider the *unnormalized* luminosity and the *unstretched* times, merely shifting the first observational data to match the start of the analytic solutions ("bang time"). This is shown in Fig. 2, using exactly the same theoretical models. The predicted bolometric luminosity ($L \sim 1.18 \times 10^{43}$ erg/s, or $L/L_\odot \sim 3.06 \times 10^9$) agrees well with that from Pereira, et al. (2013).

Unfortunately *the theoretical uncertainty in the leakage time ("effective opacity") makes the theoretical fits, while plausible, neither*

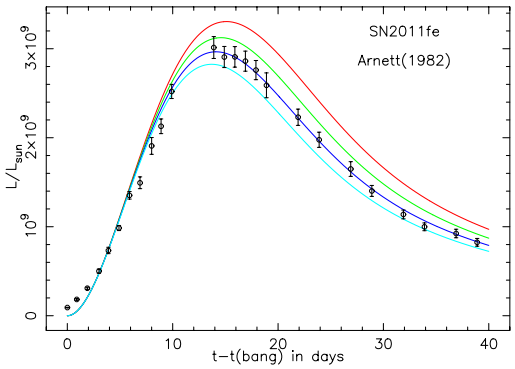

Figure 2. Comparison of bolometric luminosity from analytic models (Arnett 1982) and SN2011fe (Pereira, et al. 2013). The models are the same as in Fig. 1. For the same time of explosion, the more luminous curves peak at a later time, and hence have a larger width (Phillips 1993), as the parameter p_2 is changed (see text). Prior to peak luminosity, the theoretical curves are almost invariant under changes in p_2.

unique nor simple to interpret; see §5.2 below.

Fig. 2 shows that the light curves are almost invariant with respect to variations of the parameter p_2 prior to peak luminosity, but they do vary significantly after the peak (which shifts in time). This regularity is hidden in the conventional presentation such as shown in Fig. 1. The broader curves have higher luminosity (the Philips relation, Phillips (1993)). The variability in width is not symmetrical, and is clearly determined by the post–peak behavior, as observed by Firth, et al. (2015).

The Phillips–relation behavior seen in Fig. 2 may be due to (1) Ni having a higher opacity than Si–Ca (that is, $\kappa_{Ni} > \kappa_{SiCa}$), and (2) only Ni contributing the the radioactive heating. Hoeflich, Khoklov & Mueller (1991); Pinto & Eastman (2000b) have stressed the importance of frequency-dependent opacity and the complexity of the problem; see also discussion in §5.2. The current state of the art may be Blondin, et al. (2013). While the detailed problem is complex, the essential features of the light curves are captured by a simple leakage time (an "effective opacity" parameter which is easy to specify but difficult to calculate convincingly and uniquely).

Burning ^{12}C and ^{16}O to nuclei lying in the range ^{28}Si–^{40}Ca releases almost as much explosive energy as burning the same nuclei to ^{56}Ni ($q_{SiCa} \sim q_{Ni}$), but the ashes Si–Ca are not radioactive, and do not provide late heating. This implies that the analytic models for a thermonuclear supernova should have a connection between the explosion energy and the mean opacity (leakage time) which distinguishes between the mass of material burned to ^{28}Si–^{40}Ca and to ^{56}Ni. Thus

$$E_{sn} \approx M_{Ni}\, q_{Ni} + M_{SiCa}\, q_{SiCa} \qquad (3)$$

where q represents the appropriate energy release per unit mass of fuel burned, and

$$\kappa \approx X_{Ni}\, \kappa_{Ni} + X_{SiCa}\, \kappa_{SiCa}, \qquad (4)$$

where κ represents the opacity. It is possible to increase both the luminosity and the leakage time (width of the peak) by increasing the amount of ^{56}Ni produced (the Phillips relation), if the burning varies in degree of completeness.

2.3. *Supernovae observed by the Kepler satelite*

While the Kepler satellite does not have comparable wavelength coverage to that which became available for SN2011fe, the Kepler coverage is broadband, has high cadence in time, has small errors from statistical fluctuations, is free from multi-instrumental inconsistency, and has light curves which track the data from SN2011fe well; see Fig. 1 in Olling, et al. (2015) and Fig. 3.

The spectra of SN 2011fe in Pereira, et al. (2013) were obtained using the SuperNova Integral Field Spectrograph (Lantz et al. 2004) on the 88" telescope on Mauna Kea and are presented as fully calibrated. We convolved the spectra with the filter function for Kepler (a wide filter, $\sim 4400 - 8800$ Å)[6]. The Kepler system is not fully calibrated, so there is no measured zero point to place Kepler magnitudes on a known scale. We used a zero point similar to that for standard filters, a procedure which gives a reasonable answer, but still contains some arbitrary scaling. Even evaluating the flux directly from the spectra through the filter requires some knowledge of the calibration of the filter. We can construct a Kepler magnitude and a flux in the Kepler filter for each spectrum, that are all consistent relative to each other, but there is still an uncertain absolute scaling. Actual bolometric corrections are hard to do without calibrating the Kepler system.

As an alternative, we take the Kepler magnitude light curve of SN 2011fe, show that it

[6] http://keplerscience.arc.nasa.gov/the-kepler-space-telescope.html

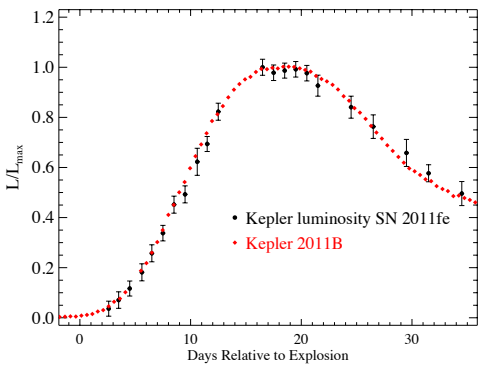

Figure 3. Comparison of the luminosity of SN 2011fe (Pereira, et al. 2013) in the Kepler filter and adjusted data (see text) based on KSN2011b (Olling, et al. 2015). The time axis was translated to match the point of explosion. We took the time of explosion for SN 2011fe from Pereira, et al. (2013) (2.6 days before the first spectrum) and from Olling, et al. (2015) for Kepler 2011b (18.1 days before maximum). The light curves presented by Pereira, et al. (2013) are also obtained by convolving filter functions with their spectra. They estimate the errors in their magnitudes using the flux calibration procedure for their spectra and we adopt the same 1σ errors per epoch.

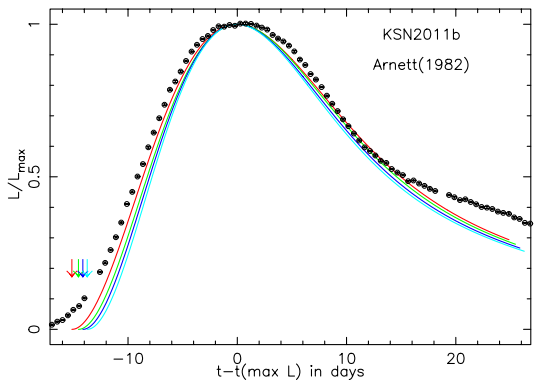

Figure 4. Comparison of bolometric luminosity from analytic models (Arnett 1982) and KSN2011b (Olling, et al. 2015), which are both smooth. The deviation of the post-peak radioactive tail may be due in part to our bolometric correction procedure, which was focused on the pre-peak and peak behavior (see text). The parameters from Table 1 were used with no adjustment.

is similar to KSN2011b, and then infer that the bolometric light curve of KSN2011b would be similar to SN2011fe. There are many caveats that need to be considered for such an inference, such as the fact that SN2011fe and KSN2011b may have different bolometric characteristics. Given the striking similarity of the two light curves in the Kepler band, though, we believe that this is a plausible inference. We take the flux and treat it as a relative luminosity (L/L_{max}); this ratio also removes concerns about absolute scaling. Fig. 3 shows the time evolution of L/L_{max} for both SN2011fe and KSN2011b.

It appears that SN2011fe and KSN2011b are similar enough that we may use this similarity in the data to establish a correspondence between the bolometric scale of SN2011fe and the Kepler supernovae.

Now that we have a calibration, how do the Kepler supernovae compare with the analytic curves? The best example, KSN2011b, from Olling, et al. (2015) is shown in Fig. 4. Again we see a deviation between observations and analytic light curves at very early times, which may be related to use of the coasting approximation. After this first deviation, the curves are strikingly similar, as the higher cadence of the Kepler data makes clear. Although the observed supernovae might not be identical, so that fitting with different theoretical parameters would be legitimate in principle, we have used exactly the same theoretical parameters as in Fig. 1 in order to illustrate just how similar these light curves seem to be.

Well past peak light (> 15 days), there is a deviation between the analytic models and our approximate bolometric conversion of the KSN2011b data. This corresponds to the "radioactive cobalt tail" and, while important, is beyond the scope of our present discussion. The deviation may be due to our procedure for bolometric correction, which was focused on the pre-peak and peak epochs.

Because of the fast cadence of observations and stability of its instrumentation, Kepler provides new information on SNIae: the smoothness of the light curve. While KSN2012b tracks SN2011fe within its error bars, the KSN2012b light curve is noticeably smoother (the error bars for KNS2012b are plotted in Fig. 4, but are so small they merely give a slightly fat dot). There is no indication of bumps due to (1) collision of ejecta with circum-supernova matter, as with SNIbn and SNIIn events, or to (2) variation in opacity due to spherical shells of different composition. SN2011fe does exhibit fluctuations consistent with its observational error bars, an issue that will resurface later (Figure 9 and §3.3).

3. A PHASE DIAGRAM FOR TYPE I SUPERNOVAE

3.1. *Time derivatives of luminosity*

We may discuss the shape of normalized light curves in terms of time derivatives, which we approximate as time–centered finite differences over three points in time:

$$dL/dt \approx \frac{1}{2}\left[\frac{L_2-L_1}{t_2-t_1} + \frac{L_1-L_0}{t_1-t_0}\right], \qquad (5)$$

and

$$d^2L/dt^2 \approx \frac{\left[\frac{L_2-L_1}{t_2-t_1} - \frac{L_1-L_0}{t_1-t_0}\right]}{\frac{1}{2}(t_2-t_0)}, \qquad (6)$$

where the subscripts indicate the sequence of observation, and the luminosities L are assumed to be normalized (as in Fig. 1 and 4). Because of the repeated differences used in the construction of Eq. 6, high quality evaluations of the luminosities are necessary to avoid a result dominated by observational error. This is especially true if the light curve is nearly linear ($dL/dt \sim$ constant). The time appears only in differences, so that the zero in time is irrelevant in defining these finite differences, although it is relevant in comparing observation and theory (centering the peak and estimating "bang" time).

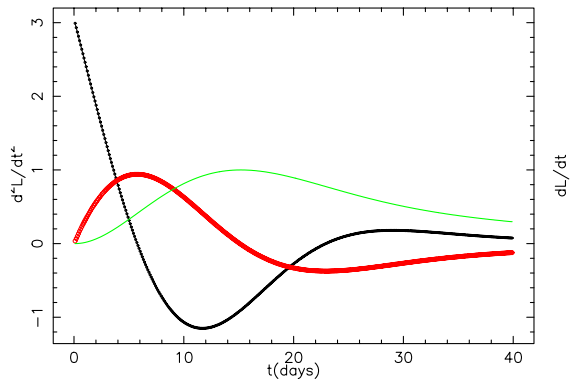

Figure 5. Time dependence of luminosity (thin green line) and first and second derivatives (thick red and medium black lines) for Type I supernovae, illustrated by the default analytic model (cyan shown in previous figures). Most variation occurs prior to maximum light (at ∼16 days).

Fig. 5 shows the variation with time of the luminosity (solid green line) and its first (thick red line) and second derivatives (medium black line) with respect to time. Most of the variation occurs early, prior to peak luminosity at ∼16 days for these analytic models. The luminosity is normalized to that at maximum light. The first derivative is expressed in units of normalized luminosity divided by time measured in units of two mean lives for ^{56}Ni decay. The second derivative uses the same units of luminosity and time. For easier interpretation the time axis is simply labeled in units of days, beginning at explosion time.

3.2. *A phase plane for Type 1 supernovae*

The rise and fall of a light curve may be represented mathematically by a piece-wise set of pairs of luminosity and time (t_0, t_1 and L_0, L_1), which corresponds to a function and its time derivative (to detect the change). More information is contained in the second derivative of luminosity with respect to time. To define a second derivative (observationally, a second-order difference) requires a third observation. Using a set of triples of data (t_0, t_1, t_2 and L_0, L_1, L_2) we may place each triple as a point in a phase plot in the dL/dt—d^2L/dt^2 plane; this is shown in Fig. 6. The final object of interest, the luminosity, is ignored at first by normalizaton; the normalized luminosity is independent of assumed distance. We may ignore the distance and focus upon the shape of the curve. This requires use of the remaining two variables, and may be plotted in a phase plane, in which the position in the plane indicates the evolution of the trajectory of the luminosity in time, from explosion to final decline.

Fig. 6 shows such a trajectory, beginning at the point labeled "bang", and moving to maximum light, after which the luminosity falls, eventually becoming the radioactive tail. The analytic model uses the coasting approximation, like the fireball model, so that "bang" occurs away from the origin ($L \sim t^2$ has a constant positive *nonzero* second derivative). As discussed earlier and in Firth, et al. (2015), higher powers of t are more realistic, so that the "bang" should occur near the origin in this plot, and asymptotically approach the curve shown.

The choice of variables emphasizes the early (pre-peak) part of the light curve; a bias indicated by the density of dots, which are equally spaced in time. The positive value of d^2L/dt^2, with a coinciding positive value of dL/dt, indicates a light curve which is 6 days (or more) prior to maximum light. Because nearer su-

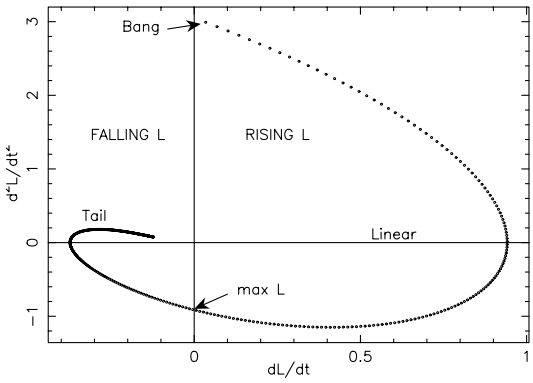

Figure 6. A Phase diagram for Type I supernovae, illustrated by analytic models (Arnett 1982). The pre-maximum evolution is emphasized with these coordinates, making the early evolution more obvious. The coasting approximation makes the earliest points deviate from observations, as shown in Fig. 1, 2, and 4. The position of the point labeled "Bang" would be at the origin in a more realistic approximation to the very early light curve (see text).

pernovae will have better statistical data, constructing a second derivative will be more reliable for those which will eventually be the brightest observational targets.

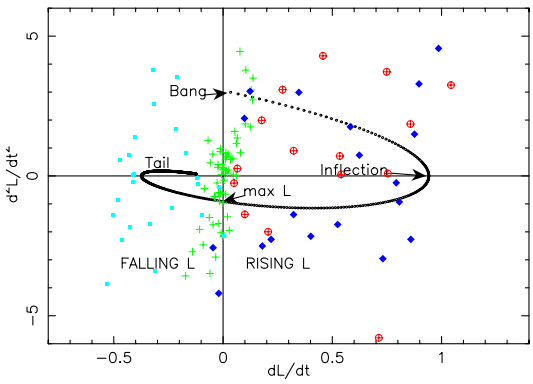

Figure 7. A Phase diagram for Type I supernovae, illustrated by analytic models (Arnett 1982) and KSN2011b data (Olling, et al. 2015). The published observational data are shown, with no smoothing. The pluses (green) are more than 18 days before maximum, and are dominated by statistical errors (no SN yet). The crossed circles (red) are from 18 to 10 days, diamonds (blue) are 10 to 0, and solid squares (turquoise) are post-maximum. There is a large scatter due to taking numerical derivatives of observational data.

In Fig. 7 are shown the data for KSN2011b (Olling, et al. 2015) in such a phase diagram. Pre-outburst data lies along the vertical axis, with post-maximum points lying to the left of this. Before the supernova is detected the data is dominated by statistical noise, which shows up as larger fluctuation in the inferred second derivative compared to the first derivative, causing the pre-outburst data to cluster around the vertical axis. The analytic model of Fig. 6 is shown for reference.

3.3. *Statistical fluctutions*

Taking finite differences of data will emphasis statistical fluctuations. However Fig. 3 indicates that at high cadence the underlying curve would be smooth. The Kepler data has an almost constant cadence, so a very simple smoothing algorithm will preserve the shape of the data by filtering the highest frequency fluctuations, which we assume to be statistical in nature:

$$\hat{y}_j = \frac{1}{2}(y_{j-1} + y_{j+1}) + \frac{1}{2}y_j, \qquad (7)$$

where the smoothed values are $\hat{y}_j$. This has a 3–point stencil, which is what is required for second derivatives; the smoothing operates on the smallest time intervals available in the data, but preserving unitarity. No data is rejected, but a smoother curve is required, as Fig. 3 implies. The smoothing algorithm (Eq. 7) is chosen as a particularly simple and transparent example; more sophisticated methods might be applied in practice, taking into account observational details. Treatment of triples of data points may be optimized for cadence and rejection algorithms.

As a test of this approach, we consider the set of sequential triplets of the KSN2011b data as an ensemble of supernova observations, with each triplet of flux measurements corresponding to a hypothetical supernova discovery. Can we identify the epoch of the discovery of each hypothetical supernovae? Yes, with surprisingly high reliability.

The KSN2011b data (Olling, et al. 2015), smoothed according to Eq. 7, is shown in Fig. 8. Of the 14 very early points, -18 to -10 days relative to maximum light, only one does not lie in the first quadrant; $\sim 93\%$ would be identified by plotting them in the phase plane. There are 19 remaining pre-maximum points, 14 of which are in the second quadrant, giving a rate of 73% correct. Very early triples have stronger evidence for a second derivative,

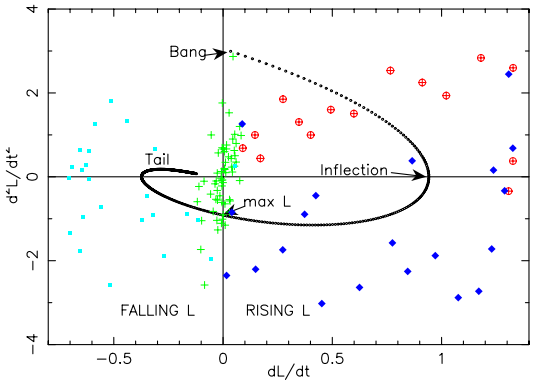

Figure 8. A Phase diagram for Type I supernovae, illustrated by analytic models (Arnett 1982) and KSN2011b data (Olling, et al. 2015). The observational data are smoothed to reduce statistical fluctuation (see text). The pluses (green) are more than 18 days before maximum, and are dominated by statistical errors (no SN yet). The crossed circles (red) are from 18 to 10 days, diamonds (blue) are 10 to 0, and solid squares (turquoise) are post-maximum. Even with the large scatter due to taking numerical derivatives of observational data, the earliest observations cluster in the first quadrant.

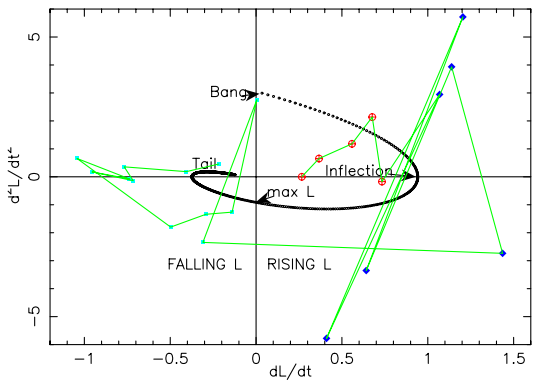

Figure 9. A Phase diagram using SN2011fe data (Pereira, et al. 2013). The observational data are *not* smoothed to reduce statistical fluctuation (see text). The crossed circles (red) are from 8 days or more prior to maximum, diamonds (blue) are from -8 to maximum, and solid squares (turquoise) are post-maximum. Even with the large scatter due to taking numerical derivatives of observational data, the first five triples of data are in the first quadrant. The data sequence is in time order, connected by a solid (green) line to visually highlight fluctuations, which we suspect may be attributed to statistical error; see Fig. 3.

which favors their identification (93% versus 73%). The Kepler data was binned with a cadence of ~ 0.5 days which is not too short to see a change, nor too long to provide good time resolution; see Fig. 5.

Use of a more sophisticated version of such an approach should allow the development of a reliable automated system for detection of good candidates for detailed follow-up observations. Although Fig. 8 has its own theoretical value, it may prove to be of most use in categorizing observational data of SNIae, and identifying promising targets early in their evolution.

Fig. 9 shows the phase diagram for SN2011fe data (Pereira, et al. 2013), *with no smoothing*. Notice the larger range of the variables than in the previous figure. The first five triples of data lie in the first quadrant, indicating a supernova more than ~ 8 days prior to maximum in this case. The earliest data points radiate from the origin, consistent with $L \propto t^n$ with $n > 2$. The next data are in the linear rise, so that the second derivative is small and thus sensitive to statistical error. This causes the diagonal jitter seen near the label "Inflection". Examination of Fig. 3 shows that this jitter corresponds to an epoch in which the SN2011fe data does show larger wiggles than the KSN2011b data. The higher cadence of the Kepler data and the greater observational consistency (a single nstrument in space) seem to be beneficial. The intercept is relatively well-defined (dL/dt) and agrees with the analytic model, but the value of d^2L/dt^2 is dominated by statistical error. Some sets of triple observations, with an even spacing of ~ 0.5 days, would make the descending light curve less sensitive to observational error.

4. OTHER SUPERNOVAE

The similarity in light curves of thermonuclear and core-collapse supernovae (Arnett 1982) suggests the hope that these procedures might be extended. How does the phase plane behave for types SNIbc? Intrinsic diferences between SNIa and SNIbc supernovae present challenges.

4.1. *SN2008D, a SNIb*

Supernova 2008D was discovered at the time of explosion, which coincided with an X-ray event due to the break-out of the supernova shock wave (Soderberg et al. 2008). This was the first successful observation of the previously predicted break-out of a supernova shock (Colgate & McKee 1969; Arnett

Table 3
Parameters for model of SN2008D

Variable	Symbol	Value
Mass ejected[a]	M_{ej}	$2.9M_\odot$
Initial ^{56}Ni	$M_{Ni}(0)$	$0.10M_\odot$
Initial radius	$R(0)$	1.0×10^{10} cm
Opacity	κ_t	0.10 cm^2 g^{-1}
Explosion energy	E_{sn}	5.0×10^{51} ergs

[a] Total stellar mass is M_{ej} plus the mass of the collapsed core for SNIb.

1971; Chevalier 1976), and to be associated with a bare core, or stripped-envelope supernova (Arnett 1977). Modjaz, et al. (2008) presented a detailed discussion of the observational data (optical, infra-red, and X-ray) of this event, and Bianco, et al. (2014) summarized the results for 64 similar events, including this one. None of the others exhibit clear evidence for break-out; such evidence might have been missed in the other supernovae. We base our discussion on the data sets in these papers, which contain a more detailed history and references.

SN2008D occurred in NGC 2770 ($D = 31 \pm 2$ Mpc) and had a peak absolute magnitude of $M_V = -17.0 \pm 0.3$ mag and $M_B = -16.3 \pm 0.4$ mag (Modjaz, et al. 2008). The rise time in the V-band was 16.8 ± 0.4 days and in the B-band 18.3 ± 0.5 days, near the long end of the range for SNIbc. The observation of the X-ray outburst determines a more precise value for the explosion time, which is of value in fitting theoretical models to the data. Integrating the observed bands, or fitting a blackbody give similar bolometric corrections, so that at 19.2 days after explosion, the bolometric luminosity peaks at $L = 10^{42.2 \pm 0.1}$ erg s^{-1} or $L = 4.12 \times 10^8 L_\odot$.

The key parameters chosen for SN2008D are given in Table 4. For comparison, Soderberg et al. (2008) gives $R_* \sim 7 \times 10^{10}$ cm, $v_{ph} \sim 0.3(E_K/M_{ej})^{1/2} \sim 11,500$ km/s, $E_K \sim (2-4)$ bethe, $M_{ej} \sim (3-5)M_\odot$ and $M_{Ni} \sim (0.05-0.1)M_\odot$. This is reasonable consistency, considering our different strategy for de-convolving the breakout and radioactively driven epochs (see below).

In order to compare bolometric light curve shapes to observational data, we employ a crude but suggestive approximation: we correct the V-band magnitudes (Bianco, et al. 2014) using the bolometric luminosity at peak light (Modjaz, et al. 2008). Instead of a constant scaling, a better approach would be to use a variable one (see Fig. 9 in Modjaz, et al. (2008), but from 10 to 30 days after outburst, the variation is not large. Moreover, the very early analytic light curves are plagued by errors due to the coasting approximation (see §2.1), so for the present we choose a simple approximation which is adequate for illustration. The nature of the error is to underestimate the luminosity from 0–10 days after outburst; the first V-band point (with our scaling, $\sim 1.4 \times 10^8 L_\odot$) is about 0.01 of the X-ray luminosity ($\sim 1.6 \times 10^{10} L_\odot$, which lasts only ~ 200 seconds, Soderberg et al. (2008)).

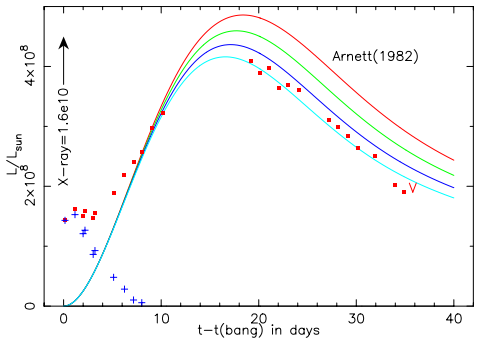

Figure 10. Scaled V-magnitudes from the Ib supernova SN2008D (Bianco, et al. 2014) compared to analytic models, using the bolometric correction at peak light of (Modjaz, et al. 2008); see text. The initial X-ray burst is 100 times brighter than the first V-band luminosities, but only lasts ~ 200 seconds. The pluses denote the differences between scaled V-band luminosities and the analytic solutions (which ignore burst behavior), and are thus an estimate (lower bound?) of the thermal luminosity of the burst.

In Fig. 10 the scaled V-band data is compared to the analytic light curves with the parameters given in Table 4, and with the same fractional variation in parameter p_2 as used previously for SN2011fe and KSN2008b. In the coasting approximation the initial radius is only relevant in that it is small; there is no shock break-out in analytic solutions which use this approximation, so that only the effects of radioactive heating are captured. Notice the excess luminosity relative to the analytic solutions for $t \leq 6$ days, which in fact is due to shock break-out and to cooling non-homologous expansion and higher moments of the radiative diffusion solutions (Arnett 1980, 1982; Pinto & Eastman 2000a). After this time the total luminosity (which is due primarily to radioactive decay) is well repre-

sented by this analytic model.

Chevalier & Fransson (2008) conclude that "a shock breakout model does not reproduce the observations in a straight-forward way"; their preferred model is a combination of breakout plus a central engine of some sort. The initial radius is a key parameter in their discussion, and it may be that there is a conflation of the initial stellar radius prior to breakout and that immediately after, which rapidly changes. A fluid-dynamic treatment will give a strongly non-homologous expansion after breakout at initially small radii (Arnett 1980), resulting in modification of density structure, radiation temperature, and radiation leakage. In particular, arguments based upon similarity solutions in an atmosphere may be questionable during this transition phase, in which an initially hydrostatic configuration (centrally condensed) changes into a Sedov-like ring structure (see §99 and Fig. 78 in Landau & Lifshitz (1959)) . This is a more acute form of the problem of luminosity evolution at early time for SNIae discussed in regard to the fireball and coasting approximations in §2.1.

Subtracting the analytic solution from the observations gives an estimate of the luminosity due to the breakout itself (discussed in Soderberg et al. (2008); Modjaz, et al. (2008)), plus the radiative relaxation which follows (Arnett 1980), and contains information about the explosion, the structure of the progenitor, and possible effects of a central engine[7]. The blue pluses represent an estimate of the luminosity due to this early burst alone; it is constructed by subtracting the analytic solution from the shifted V-band observations, and thus is an estimate of the *minimum* luminosity. A definitive comparison requires a bolometric light curve derived from the observations, but Fig. 10 illustrates a fundamental difference in early light curves between SNIa, and SNIb (see Fig. 2 and 4).

For SN2008D, the early thermal luminosity occurs during the epoch at which the phase diagram does work for SNIae, which have a negligible thermal luminosity bump (perhaps due to smaller progenitor radii). The interpretation of the early light curve may be further complicated by variations in the initial radii of the progenitor stars. All SNIb may not be like the best-observed one; see Fig. 13 in Bianco, et al. (2014).

[7] It is expected that a SNIb contains a condensed core (neutron star or black hole); the question is precisely what robust information the early light curve contains about a central engine.

4.2. *SNII*

SNII light curves are dominated by light from the shock heating of an extended (red giant) envelope which is rich in hydrogen (Falk & Arnett 1973; Arnett & Falk 1976; Falk & Arnett 1977; Falk 1978). This implies that the first light would quickly become characteristic of shock emergence in low density plasma, merging into a recombination front at the photosphere (Woosley & Weaver 1986). Because of the quicker rise (the shock breakout is faster than decay of ^{56}Ni), advance warning is more difficult to attain. As with SN1987A, neutrinos from core collapse would be the first messengers, which are followed after the time interval required for the shock to travel through the envelope, by hard radiation associated with shock emergence (Arnett 1988). Gravitational waves should be another early messenger, but both neutrino and gravitational wave detection require the core-collapse supernova to be exceptionally close.

SNII are prone to hydrodynamic instabilities (Rayleigh-Taylor and Richtmeyer-Meshkov), both during the explosion and during entrainment of circumstellar material (Falk & Arnett 1973, 1977; Fryxell, Arnett & Müller 1991; Müller, Fryxell, B. & Arnett, D. 1991). This has been incorporated into supernova models only in a crude, one-dimensional (1D) way, but has 3D consequences observable in young supernova remnants (Arnett & Meakin 2016).

5. OUTSTANDING ISSUES

5.1. *Relevant parameters*

While the analytic solutions give excellent representations of the observations, it is desirable to further restrict the range of parameters by improving the underlying physics. These analytic models have four parameters: explosion energy, mean opacity (leakage time), Ni mass, and ejected mass. Specifying that the heating source is dominated by the ^{56}Ni decay chain fixes the nuclear parameters to measured values.

The explosion energy and the ejected mass affect the leakage time through the velocity. The Ni mass affects the leakage time through the opacity, and the explosion energy for purely thermonuclear supernovae through

the degree of burning (§2.2). Additional constraints will further reduce the degrees of freedom (e.g., independent measurement of the velocity field, identification of a pure thermonuclear explosion, independent constraints on the circum-supernova medium (CSNM), etc.).

5.2. *Leakage time*

The analytic solutions for the bolometric light curve require specification of a rate at which thermal energy leaks from the ejected mass; this is quantified by a "leakage time", that is, the mean time for a typical thermal photon to escape. This is estimated by a radiative diffusion model, involving the integrated effect of the Rosseland-mean opacity over structure and time. Although the local opacity will vary sensitively with the density, temperature and photon frequency, the leakage time integrates over these effects (Pinto & Eastman 2000b), giving a smoother time variation of global properties, as seen in the observations of KSN2011b (Fig. 4).

The term "opacity" in the analytic solutions is a placeholder for a *leakage time*. This "effective opacity" is a constant (for analytic simplicity) which approximates the same leakage rate for radiative energy as a physically correct simulation would (in practice, this may only mean that the choice of effective opacity fits the observations). The leakage time is determined by the fastest paths of escape, so the "opacity" represents a minimum value, and this may be why interesting light curves result from values near the electron scattering value.

A further advantage of the idea of a leakage time is that it allows a smooth transition from a spherical diffusion model to a filamentary emission model appropriate to a supernova remnant. This allows us to mitigate the complex problem of the detailed nature of the recession of the photosphere through a clumpy, heterogeneous 3D medium. The heating rate simply tracks the gamma-ray and positron deposition rate at late time, so there is no longer any delay in escape of thermal photons.

Table 4 shows the values of selected variables at maximum light for the analytic models presented earlier for SN2011fe. The temperatures lie in the range 1×10^4 K to 2×10^4 K, which are commonly found in normal stars. Because of the large radiative conductivity the SN has a relatively shallow temperature gradient.

Unlike the temperatures, the densities, of order 3×10^{-13} g cm^{-3}, are considerably lower than encountered in stellar atmospheres. These low densities suggest the question: how valid is the assumption of collisional equilibrium? As discussed in Pinto & Eastman (2000b), $v \ll c$ implies that collisional equilibrium is difficult to attain in supernovae, and thermal equilibrium comes from radiative interactions.

For a radius $R \sim 1 \times 10^{15}$ cm, the light travel time is $t_c \sim 3 \times 10^4$ seconds, or about 8 hours. In contrast, even without scatter, the travel time for electrons (which, although slow, are still faster than ions) would be $t_e \sim 10^9$ seconds, or 30 years, which is much longer than the rise times of 15 to 20 days. Because electrons will interact with ions and magnetic fields, their trajectories will not be straight, and their travel times will be much longer than this. Photons must provide whatever coupling there is across a supernova; there is no collisionally equilibrated thermal bath as is traditionally assumed in stellar atmosphere theory.

Photons are bosons, so we consider a Bose-Einstein gas not in equilibrium (Landau & Lifshitz 1969). A dilute radiation field would correspond to a finite chemical potential, skewing the equilibrium distribution from black-body to Bose-Einstein. If fluorescence can provide sufficient photon splitting, the distribution approaches a black-body (Bose-Einstein with zero chemical potential), as discussed in Pinto & Eastman (2000b).

5.3. *Physical opacity*

The opacity depends upon the density, temperature, composition, and photon energy. To illustrate the effects of non-constant opacity, we consider a toy model, but one which includes some of these effects. We consider iron as a representative composition for illustration. Figure 11 shows the logarithm of the Fe opacity as a function of photon energy, for various combinations of temperature and density. These opacities are produced by the OPLIB database team (Magee et al. 1995), extended with new calculations courtesy of C. Fontes to produce the opacities needed at low densities.

We explore some consequences of the opacity variation with a numerical model: we use a simplified "leakage scheme", assuming a single opacity for the transport, but allowing the opacities to vary dramatically with photon energy, as shown in Fig. 11. For leak-

Table 4
Some variables at maximum light for analytic models of SN2011fe

Light curve color	red	green	blue	turquoise
Explosion time (d)	−15.09	−14.57	-14.11	-13.69
$-m_{bol}$ at peak	19.08	19.02	18.96	18.91
Optical depth	419	449	479	509
ρ (g cm^{-3})	3.32×10^{-13}	3.69×10^{-13}	4.07×10^{-13}	4.45×10^{-13}
$T_c/(10^4$ K)	1.81	1.85	1.89	1.92
$T_{eff}/(10^4$ K)	1.03	1.03	1.04	1.04

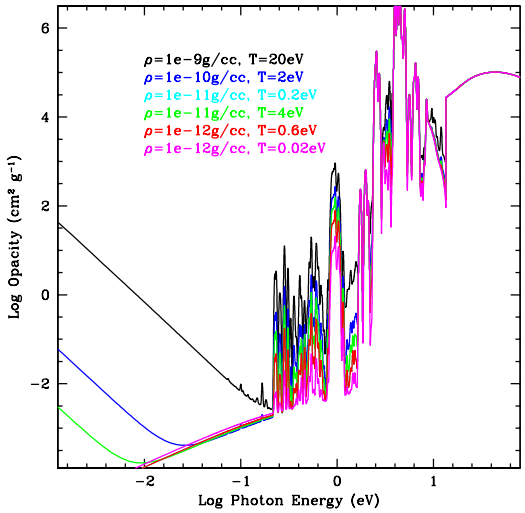

Figure 11. Logarithm of Fe opacity as a function of photon energy for various combinations of density and temperature using an extension (courtesy C. Fontes) of the OPLIB database(Magee et al. 1995). Note that as the ejecta expand (and the density and temperature decrease), the opacity in a given band can both decrease and increase.

age schemes, the transport is dominated by the dips in the opacity, not the peaks. The energy at which these dips occur depends on both the temperature and density of the supernova ejecta. The leakage opacity may vary both up and down as the ejecta expands, ranging within the visible bands from below $0.001\,\mathrm{cm}^2\mathrm{g}^{-1}$ to above $10\,\mathrm{cm}^2\mathrm{g}^{-1}$.

To better understand some of the effects of these variable opacities, we have implemented an opacity switch in the simplified transport code (Bayless, et al. 2013) that allows the opacity to move up or down by an order of magnitude as the temperature drops below $1\,\mathrm{eV}$ (1.16×10^4K). Figure 12 shows three light curves: (1) a standard model assuming $\kappa = 0.1$, as well as the opacity switch that increases (2) and decreases (3) the opacity. These light-curves demonstrate the sensitivity to changes in the opacity.

The wiggles in the light curve from the toy model and the observations of SN2011fe are roughly at the same size. However, the data from KSN2011b has much smaller error bars and is much smoother (Fig. 3, 4, 7, and 9). *This smoothness is an important constraint upon theoretical models.* With a full transport solution but in spherical symmetry, we might expect opacity variation with radius to produce observable features in the light curve, which are not noticeable in KSN2011b.

In constructing numerical light curves it is traditional to mix the composition in initial models; e.g., see Dessart, et al. (2012). Such "boxcar" mixing contrasts with plume mixing expected from physical mechanisms such as the Rayleigh-Taylor instability. This "boxcar mixing" has a 1D, spherically symmetric geometry, unlike the 3D, filamentary geometry seen in young supernova remnants. The better alternative of NLTE radiative transfer in 3D seems to be beyond present-day computational capacity.

Given the sensitivity to opacity, how do light curves become as smooth as observed by Kepler (Olling, et al. 2015)? Several effects conspire to smooth the light curves: (1) the radiative diffusion operator strongly smooths variations in temperature, (2) fluid-dynamic instabilities strongly mix the composition and density in a global sense, (3) large mean-free-paths sample disparate conditions, tending to average them, and (4) doppler shifts smooth variations in frequency space.

Besides these issues and those discussed in Blondin, et al. (2013); Dessart, et al. (2015), there are the difficulties associated with non–spherical variation inevitably resulting from instabilities in the explosion. Theoretical models of supernovae which are spherically

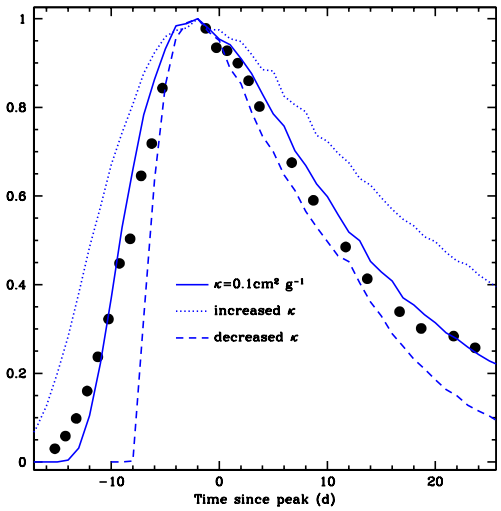

Figure 12. Comparison of bolometric luminosity from SN2011fe (Pereira, et al. 2013) using our diffusion code with 3 opacity prescriptions: constant: $\kappa = 0.1\,cm^2\,g^{-1}$ (solid), increase at low temperatures: κ increases to $1\,cm^2\,g^{-1}$ below 1 eV (dotted), decrease at low temperatures: κ decreases to $0.01\,cm^2\,g^{-1}$ below 1 eV (dashed). Raising the opacity broadens the light-curve, decreasing the light-curve narrows the light-curve. These explosions assume an explosion mass of $1.4\,M_\odot$, an explosion energy of 1.3×10^{51} erg and a nickel mass of $0.6\,M_\odot$

symmetric, can have no angular resolution to deal with this broken symmetry. Observed young supernova remnants have a pronounced filamentary structure, a heterogeneity which may have developed during this epoch of instability.

Unmixed numerical models (1D) represent a limiting case; analytic models (1 zone; using separation of variables) represent another.

Until these issues are convincingly resolved, the leakage time should be considered to be an adjustable parameter, constrained by observation, but not yet one precisely founded in experiment and simulation.

5.4. *Radioactivity and Maximum Light*

It has been shown, for one-zone models (Arnett 1979), and for solution by separation of variables (radius and time) (Arnett 1982), that for constant opacity and radioactive heating by ^{56}Ni and ^{56}Co decay, *the luminosity from radioactive heating equals that for radiative diffusion at maximum light.* , so

$$L_{peak} = M\epsilon_{NiCo}(t_{peak}). \tag{8}$$

Here we present a new derivation which is more concise, general, and hopefully clearer.

The luminosity due to radiative diffusion may be written as

$$L = aT^4R^3/\tau_{diff}, \tag{9}$$

where

$$\tau_{diff} \sim \kappa M/\beta cR, \tag{10}$$

and $\beta \approx 13.7$ is a dimensionless form factor from integration of the diffusion equation over space; see also Eq. 2. It includes the geometric factor for spherical geometry, and is very slowly varying with mass-density structure; see Table 2 and §VI in Arnett (1980).

At any extremum in L, either a peak or a dip, $dL/dt = 0$. The time derivative of Eq. 9 is

$$d\ln L/dt = 4d\ln T/dt + 4d\ln R/dt - d\ln\kappa/dt. \tag{11}$$

For a slowly-varying escape time, the term $d\ln\kappa/dt$ will be small; see discussion in §5.2 and 5.3. This is also consistent with the good fits to the light-curve data shown in Fig. 1, 2, 3 and 4 above.

A second constraint on the luminosity is first law of thermodynamics, which may be written after spatial integration as

$$L/M \sim \epsilon(t) - dE/dt - PdV/dt. \tag{12}$$

For homologous expansion (Hubble flow)

$$d\ln V/dt = 3d\ln R/dt$$

and for a radiation-dominated plasma,

$$E = 3PV = aT^4V,$$

so

$$dE/dt + PdV/dt = E(4d\ln T/dt + 4d\ln R/dt). \tag{13}$$

This requires a 3D simulation of high resolution to compute accurately, but deviations from Hubble flow may be thought of as heating from an inelastic collision of the supernova ejecta with surrounding matter. Using Eq. 11 and 13 we have

$$L/M \sim \epsilon(t) - E(d\ln L/dt + d\ln\kappa/dt). \tag{14}$$

At any extremum in L, $dL/dt = 0$, so at that time we have

$$L/M = \epsilon - E\,d\ln\kappa/dt, \tag{15}$$

for *any heating rate* ϵ. *This will be true at multiple peaks and at dips as well.* This is a more general form of Eq. 8.

Heating from other causes would have the same qualitative effects as radioactive heating. The first peak in SN2008D (Fig. 10) may be attributed to such compressional heating as the supernova shock break-out occurs. Multiple-peaked light curves like SN2016gkg (Tartaglia, et al., 2016) may also be interpreted in this way.

6. CONCLUSION

A detailed comparison of analytic light curves for Type Ia supernovae to observational data shows both good agreement and subtle differences (Pereira, et al. 2013; Olling, et al. 2015; Firth, et al. 2015). The very early light curves deviate from the "fireball" and the "coasting" model ($L \propto t^2$), which probably indicates the presence of dynamic activity not captured by those simplifications. However, both the analytic light curves and the data are distinctly non-symmetric relative to maximum light: the approach to maximum is insensitive to the parameter $p_2 = \tau_{Ni}/\tau_d$ (the Phillips relation) while the opposite is true after maximum.

We estimate a bolometric scale for the Kepler supernovae (Olling, et al. 2015) by using the data from SN2011fe (Pereira, et al. 2013), and suggest that the high cadence, low statistical error, and smoothness of the Kepler data severely constrains spherically symmetric theoretical models, requiring realistic 3D mixing.

The analytic models use the assumption of constant opacity to estimate a leakage time (§5.2), which is consistent (at least) with a global mixing ("overturn") in the explosion. This is suggested on other grounds: it is consistent with numerical simulations as well as the deep connection between Rayleigh-Taylor instabilities, Richtmeyer-Meshkov instabilities, and frozen-out turbulent convection, as well as observations of young supernova remnants; see Arnett & Meakin (2016).

The light-curve shape is independent of distance, and can provide an indication of the phase of newly–discovered supernovae of Type Ia. For the first ~ 6 days, the second time derivative is positive, $d^2L/d^2t > 0$, so that three separate observations of short cadence (~ 0.5 days) over this time are *mathematically sufficient to signal a type Ia supernova at least ten days prior to maximum.* A phase plane diagram is introduced which allows easy identification of early phases of supernova light curves. Because of the repeated differences used in the construction of approximations to second derivatives, Eq. 6, high quality evaluations of the luminosities are necessary to avoid a result dominated by observational error, especially during the almost linear part of the rise in light. The procedure does not require bolometric data in principle, but should work for well-chosen photometry that mirrors the *shape* of the pre-maximum bolometric light curve.

In summary:

1. There is excellent agreement between the best SNI bolometric data and analytic models.

2. The best very early SNIa data shows the inadequacy of both the fire-ball and the coasting approximations (which are not required for the analytic models).

3. A phase plot analysis, using dL/dt and d^2L/dt^2, may be effective for observational identification of early supernovae of type Ia. Survey telescopes such as LSST will discover many more new transients than can be studied in detail by followup telescopes (Najita, et al. 2016). By using these identifiers, supernovae which best merit detailed followup can be determined.

4. The phase plot analysis is complicated for SNIbc by non-homologous flow at and after shock break-out.

5. Spectrapolarimetry (e.g., Porter, et al. (2016); Mauerhan, et al. (2015)) can now provide new and important insight into the incomplete mixing predicted by 3D simulations to occur in supernovae (Arnett & Meakin 2016).

We wish to thank the Kepler team for providing a machine-readable copy of their data for KSN2011b,c and KSN2012a, Federica Bianco for machine-readable data for SN2008D, Chris Fontes for his calculations of Fe opacity at low density, and Gautham Narayan and Charles Kilpatrick for interesting discussions of their supernova work. We thank the Theoretical Astrophysics Program (TAP) at the University of Arizona, and Steward Observatory for support.

Table 5
Nuclear physics data[a]

Variable	Symbol	Nucleus	Value
Half-life	$\tau_{\frac{1}{2}}$	^{56}Ni	6.075 days
		^{56}Co	77.236 days
Total gamma energy	E_γ	^{56}Ni	1.750 MeV
		^{56}Co	3.610 MeV
Positron KE	$E_{\beta+}$	^{56}Co	0.120 MeV
Energy release rates	ϵ_{Ni}	^{56}Ni	3.9805×10^{10} erg/g/s
	$\epsilon_{Co}(\gamma)$	^{56}Co	6.4552×10^{9} erg/g/s
	$\epsilon_{Co}(\beta^+)^b$	^{56}Co	2.1458×10^{8} erg/g/s

[a] Slightly updated and extended version of Nadyozhin (1994), using the NNDC Chart of Nuclides `www.nndc.bnl.gov/chart`.
[b] Mean kinetic energy of positron emission; positrons are assumed to slow before annihilation, and these gamma rays are assumed to escape.

APPENDIX

NUCLEAR DATA

The data for the nuclear decay of ^{56}Ni and ^{56}Co in the analytic light curves is documented in Table 5.

VERY EARLY LIGHT CURVES

The development of a supernova explosion may be divided in time by the moment of shock outburst at the surface. Before that the internal hydrodynamics of instabillity and explosion occur; after that the ejected matter rearranges itself into a homologous expansion, barring interaction with significant amounts of surrounding plasma (however see Falk & Arnett (1977); Chatzopoulos, Wheeler & Vinko (2012); Smith (2014)). At a time t shortly after the outburst at $t = 0$, the radius of the supernova is approximately

$$R(t) \approx R(0) + v_{sc}(0)t + a_{sc}(0)(t^2/2). \tag{B1}$$

The fluid velocity behind the shock is $v_{sc}(0)$, which is non-zero. Supernovae are strongly radiation-dominated, so we take the acceleration term to be dominated by radiation stress, giving

$$a_{sc}(0) \sim -\frac{1}{\rho}\frac{dP_{rad}}{dr}. \tag{B2}$$

For radiative diffusion

$$F_{rad} = -\frac{c}{\rho\kappa}\frac{dP_{rad}}{dr}, \tag{B3}$$

so

$$a_{sc}(0) \sim \frac{c}{\kappa}F_{rad} = \frac{c}{\kappa}\frac{L(0)}{4\pi R(0)^2}, \tag{B4}$$

For a given effective temperature, the luminosity rises as the surface area, $4\pi R(t)^2$, which rises faster than t^2, as discussed in §2.1.

Time integration of the analytic light curves can be modified to include a changing acceleration $a_{sc}(t)$, thus avoiding the coasting and the fireball approximations. This acceleration and the velocity $v_{sc}(t)$ may be used with early observations to infer the size of the progenitor at shock break-out, as well as solving the $L \sim t^2$ problem at early times.

REFERENCES

Abarzhi, S. I., 2010, Phil. Trans. R. Soc. A, 368, 1809

Abarzhi, S. I., & Rosner, R., 2010, Physica Scripta, T142, 014012
Arnett, W. D., 1971, ApJ, 163, 11
Arnett, W. D. & Falk, S. W., 1976, ApJ, 210, 733
Arnett, W. D., 1977, 8th Texas Symposium on Relativistic Astrophysics, 302, Ann. N. Y. Acad. Sci., 90
Arnett, W. D., 1979, ApJ, 230, L37
Arnett, W. D., 1980, ApJ, 237, 541
Arnett, W. D., 1982, ApJ, 253, 785
Arnett, W. D., 1988, ApJ, 331, 377
Arnett, D., 1996, *Supernovae and Nucleosynthesis*, Princeton University Press, Princeton NJ
Arnett, W. D. & Meakin, C., 2011, ApJ, 733, 78
Arnett, W D., & Meakin, C., 2016, Reports of Prog. Phys., 79, 10, 102901
Arnett, W. D., Meakin, C. A., Viallet, M., Campbell, S. W., Lattanzio, J. C. & Mocák, M., 2015, ApJ, 809, 30
Bayless, A. J., Even, W., Frey, L. H., Fryer, C. L., Roming, P. W. A., Young, P. A. 2015, ApJ, 805, 98
Bianco, F. B., Modjaz, M., Hicken, M., Friedman, A., Kirshner, R. P., Bloom, J. S., Challis, P., Marion, G. H., Wood-Vasey, W. M., & Rest, A., 2014, ApJS, 213, 19
Blondin, S., Dessart, L., Hillier, D. J., Khokhlov, A. M., 2013, MNRAS, 429, 2127
Chatzopoulos, E., Wheeler, J. C., & Vinko, J., 2012, ApJ,, 746, 121
Chevalier, R. A., 1976, ApJ, 208, 826
Chevalier, R. A. & Kirshner, R. P., 1978, ApJ, 219, 931
Chevalier, R. A., & Frasson, C., 2008, ApJ, 683, L135
Clayton, D. D., 1968, Principles of Stellar Evolution and Nucleosynthesis, McGraw-Hill, New York
Colgate, S. A., 1969, ApJ, 157, 623
Colgate, S. A., Petschek, A. G., & Kriese, J. T., 1980, ApJ, 237, L133
Dessart, L., Hillier, D. J., Chenngdong Li, & Woosley, 2012, MNRAS, 424, 2139
Dessart, L., Hillier, D. J., Woosley, S. E., Livne, E., Waldman, R., Yoon, S-C., Langer, N., 2015, MNRAS, 453, 2189
Dessart, L., Hillier, D. J., Woosley, S. E., Livne, E., Waldman, R., Yoon, S-C., Langer, N., 2016, MNRAS, 458, 1618
Falk, S. W., 1978, Appl. Phys. Lett., 226, L133
Falk, S. W., & Arnett, W. D., 1973, ApJ, 180, L65
Falk, Sydney W. & Arnett, W. David, 1977, ApJS, 33, 515
Fesen, R. A., & Milisavljevic, D., 2016, ApJ, 818, 17
Firth, F. E., Sullivan, M., Gal-Yam, A., Howell, D. A., Maguire, K., Nugent, P., Piro, A. L., Baltay, C., Feindt, U., Hadjiyksta, E., McKinnon, R., Ofek, E., Rabinoowitz, D., Walker, E. S., 2015, MNRAS, 446, 3895
Fryxell, B. A., Arnett, W. D., & Müller, E., 1991, ApJ, 367, 619
Hoeflich, P., Khoklov, A., & Müller, E., 1991, A&A, 248, L7
Kirshner, R. P. & Chevalier, R. A., 1977, ApJ, 218, 142
Landau, L. D. & Lifshitz, E. M., 1959, Fluid Mechanics, Pergamon Press, London.
Landau, L. D. & Lifshitz, E. M., 1969, Statistical Physics, 2nd Ed., Addison–Wesley, Reading MA.
Lantz, B., Aldering, G., Antilogus, P., et al. 2004, Proc. SPIE, 5249, 146
Magee, N. H., Abdallah, J., Jr., Clark, R. E. H., Cohen, J. S., Collins, L. A., Csanak, G., Fontes, C. J., Gauger, A., Keady, J. J., Kilcrease, Merts, A. L. 1995, in ASP Conf. Ser. 78, Astrophysical Applications of Powerful New Databases, ed. S. J. Adelman & W. L. Wiese (ASan Francisco, CA: ASP). 51
Landau, L. D. & Lifshitz, E. M., 1969, Statistical Physics, 2nd Ed., Addison–Wesley, Reading MA.
Mauerhan, J., Williams, G. G., Leonard, D. C., Smith, P. S., Filippenko, A. V., Smith, N., Hoffman, J. L., Huk, L., Clubb, K. I., Silverman, J. M., Cenko, S. B., Milne, P., Gal-Yam, A., Ben-Ami, S., 2015, MNRAS, 453, 4467
Modjaz, M., Li, W., Butler, N., et al., 2009, ApJ, 702, 226
Müller, E., Fryxell, B. & Arnett, D., 1991, A&A, 251, 505
Munari, U., et al., 2013, New Astronomy, 20, 30
Nadyozhin, D. K., 1994, ApJS, 92, 527
Najita, Joan; Willman, Beth; Finkbeiner, Douglas P.; Foley, Ryan J.; Hawley, Suzanne; Newman, Jeffrey A.; Rudnick, Gregory; Simon, Joshua D.; Trilling, David; Street, Rachel; and 41 coauthors, 2016, Maximizing Science in the Era of LSST: A Community-Based Study of Needed US Capabilities, 2016arXiv161001661N
Olling, R., Mushotzky, R., Shaya, E., Rest, A., Garnavich, P., Tucker, B., Kasen, D., Margheim, S., & Filippenko, A., 2015, Nature, 521, 332
Pereira, R., Thomas, R. C., Aldering, G., et al., 2013, A&A, 554, A27
Phillips, M., 1993, BAAS, 182, 2907
Pinto, P. A., & Eastman, R., 2000a, ApJ, 530, 744
Pinto, P. A., & Eastman, R., 2000b, ApJ, 530, 757
Pinto, P. A., & Eastman, R., 2000c, New Astronomy, 6, 307
Piro, A. L., & Nakar, E., 2013, ApJ, 769, 67
Porter, A., Leising, M., Williams, G., Milne, P., Smith, P., Smith, N., Bilinski, C., Hoffman, J., Huk, LL.,, Leonard, D., 2016, ApJ, 828, 24
Riess, A., 1999, AJ, 118, 2675
Smith, Nathan,, 2014, ARA&A, 785, 82
Smitka, M., et al., in preparation

Soderberg, A. M., Berger, E., Page, K. L, et al. 2008, Nature, 453, 469
Swisher, N. C., Kuranz, C. C., Arnett, D., Hurricane, O., Remington, B. A., Robey, H. F., & Abarshi, S. I., 2015, Physics of Plasmas, 22, 102707
Tartaglia, L., Fraser, M., Sand, D. J., Valenti, S., Smartt, S. J., McCully,, C., et al., 2016, arXiv: 1611.00419v1
Turuan, J. W., Arnett, W. D., & Cameron, A. G. W., 1967, Can. J. Phys., 45, 231
Valenti, S., Benetti, S., Cappellaro, E., Patat, F., Mazzali, P., Turatto, M., Hurley, K., Maeda, K., Gal-Yam, A., Foley, R. J., Filippenko, A. V., Pastorello, A., Challis, P., Frontera, F., Harutyunyan, A., Iye, M., Kawabata, K., Kirshner, R. P., Li, W., Lipkin, Y. M., Matheson, T., Nomoto, K., Ofek, E. O., Ohyama, Y., Pian, E., Poznanski, D., Salvo, M., Sauer, D. N., Schmidt, B. P., Soderberg, A., & Zampieri, L., 2008, MNRAS, 383, 1485
Woosley, S. E. & Weaver, T. A., 1986, ARA&A, 24, 205
Zheng, W., et al., ApJ, 778, L15
Zingale, M., Nonaka, A., Almgren, A. S., Bell, J. B., Malone, C. M., & Woosley, S. E., 2011, ApJ, 740, 8